catalysts

MDPI

Article

Ambient Temperature CO Oxidation Using Palladium–Platinum Bimetallic Catalysts Supported on Tin Oxide/Alumina

James K. Aldridge [1], Louise R. Smith [1], David J. Morgan [1], Albert F. Carley [1], Mandy Humphreys [2], Michael J. Clarke [2], Patricia Wormald [2], Stuart H. Taylor [1,*] and Graham J. Hutchings [1,*]

[1] Cardiff Catalysis Institute, School of Chemistry, Cardiff University, Main Building, Park Place, Cardiff CF10 3AT, UK; jameskaldridge@gmail.com (J.K.A.); SmithL50@cardiff.ac.uk (L.R.S.); morgandj3@cardiff.ac.uk (D.J.M.); Carley@Cardiff.ac.uk (A.F.C.)

[2] Molecular Products, Parkway, Harlow Business Park, Harlow, Essex CM19 5FR, UK; haroldtheplatypus@gmail.com (M.H.); mikejclarke@btinternet.com (M.J.C.); pw@molprod.com (P.W.)

* Correspondence: taylorsh@cardiff.ac.uk (S.H.T.); hutch@cardiff.ac.uk (G.J.H.); Tel.: +44-(0)29-2087-4062 (S.H.T.); +44-(0)29-2087-4059 (G.J.H.)

Received: 8 September 2020; Accepted: 16 October 2020; Published: 22 October 2020

Abstract: A series of Pt-based catalysts were synthesised and investigated for ambient temperature CO oxidation with the aim to increase catalytic activity and improve moisture resistance through support modification. Initially, bimetallic PtPd catalysts supported on alumina were found to exhibit superior catalytic activity compared with their monometallic counterparts for the reaction. Following an investigation into the effect of Pt/Pd ratio, a composition of 0.1% Pt/0.4% Pd was selected for further studies. Following this, SnO_2/Al_2O_3 supports were synthesised from a variety of tin oxide sources. Catalytic activity was improved using sodium stannate and tin oxalate precursors compared with a traditional tin oxide slurry. Catalytic activity versus tin concentration was found to vary significantly across the three precursors, which was subsequently investigated by X-ray photoelectron spectroscopy (XPS) and energy-dispersive X-ray spectroscopy (EDX).

Keywords: catalytic oxidation; carbon monoxide; palladium; platinum; tin oxide; alumina

1. Introduction

Catalytic carbon monoxide oxidation is one of the simplest oxidation reactions, but it has been extensively studied due to the numerous environmental and industrial applications [1–3]. Hopcalite catalysts, comprising copper and manganese oxides, are widely utilised for CO oxidation due to their excellent activity at ambient temperatures and low cost [4,5], although they can be sensitive to water vapour and thus prone to deactivation in the presence of moisture [6]. Supported platinum group metals (PGMs) are highly active in catalytic oxidation reactions [7–10], exhibiting activity for CO oxidation at ambient temperatures; however, the PGM content should be minimised due to the high cost and tendency for CO self-poisoning [11,12].

Numerous metal oxides have been investigated as supports for Pt- and Pd-based CO oxidation catalysts, with higher activities typically observed over reducible supports, such as CeO_2, TiO_2 and Fe_2O_3, compared with non-reducible oxides, such as Al_2O_3 and SiO_2 [13–20]. SnO_2 has been demonstrated to be an efficient support for low temperature CO oxidation catalysts. Bond et al. demonstrated the superior activity of Pd/SnO_2 compared with Pd/SiO_2 and Pd/Al_2O_3, which was attributed to the spillover of CO and O_2 from the metal to the support [21]. The high activity of Pd/SnO_2 and Pt/SnO_2 catalysts have also been reported by numerous authors [21–27], with several

mechanisms proposed to account for the enhanced catalytic activity. Sheintuch et al. also suggested a spillover mechanism, although it was considered to be restricted to CO [24]. An alternative explanation was proposed by Grass et al. whereby O_2 adsorption on SnO_2 followed by migration to the Pt/SnO_2 interface was considered to be responsible for the high activity [23]. A number of studies by Margitfalvi et al. using supported PtSn catalysts showed the formation of a tin–platinum alloy, with Sn^{4+}–Pt ensemble sites identified as the active species [28–31].

Bimetallic PtPd/Al_2O_3 catalysts were demonstrated to exhibit superior catalytic activity by Hazlett et al. when compared with their monometallic counterparts [32]. The most active catalysts were found to be 1:1 PtPd/Al_2O_3 and 1:3 PtPd/Al_2O_3. The lower activities obtained over Pt/Al_2O_3 and the Pt-rich bimetallic catalyst was attributed to the increased sensitivity of Pt to CO self-poisoning [33], evidenced by the presence of CO–M–CO species observed via DRIFTS. The proportions of linearly, doubly and triply bound CO were calculated over the different catalysts. A strong correlation was found to exist between low temperature CO activity and the proportion of CO–M–O species observed, whereas CO–M–CO species were correlated to the poisoning of the catalyst surface by CO. The monometallic Pd catalyst was shown to be inhibited by surface carbonate formation.

Whilst Pt/SnO_2 and Pd/SnO_2 are both active as ambient temperature CO oxidation catalysts, the surface area of the support is generally low [22,34], which can result in poor metal dispersion. On the other hand, alumina is extensively used as a catalyst support due to its high surface area and excellent thermal stability. The impregnation of alumina with stannic oxide to produce SnO_2/Al_2O_3 materials can provide a catalyst support with superior catalytic activity due to the combination of active oxygen species from SnO_2 and the high surface area of Al_2O_3, resulting in Pt and Pd catalysts with enhanced activity [25].

The preparation of PtPd/SnO_2/Al_2O_3 catalysts using three different tin sources is compared herein. Initially, mono- and bimetallic PtPd/Al_2O_3 catalysts, prepared through an electrostatic adsorption (EA) technique, were investigated for CO oxidation. Following identification of the most efficient bimetallic composition, the effect of tin oxide addition was investigated, and PtPd/SnO_2/Al_2O_3 catalysts were prepared by various methods. In addition to the traditional tin oxide method, catalysts are also prepared with sodium stannate and tin oxalate; the latter involves a combustion method following treatment with a weak hydrogen peroxide solution, thus producing a catalyst free of surface contaminants.

2. Results

2.1. CO Oxidation Using Bimetallic PtPd Catalysts Supported on γ-Alumina Spheres

We investigated the ambient temperature oxidation of CO for monometallic eggshell catalysts prepared using γ-alumina spheres. Under the reaction conditions used, the γ-alumina spheres showed no activity for CO oxidation. The results for time online with different metal loadings are given in Figures 1 and 2. As the metal loading increased, so did the catalyst activity. However, when the two metals were combined, there was an enhancement in activity (Figure 3). The data in Figure 3 are for 1:1 mass ratio of the two metals, so we then investigated the effect of the ratio of the two metals. A series of Pt- and Pd-impregnated catalysts were prepared. Pd loadings of 0.1 wt % to 0.7 wt % and Pt of 0.04 wt % to 0.16 wt % were deposited onto γ-Al_2O_3 spheres to find the most efficient CO oxidation catalyst. Varying the amount of Pd at constant Pt had a distinct effect on CO oxidation activity (Figure 4). The addition of small amounts of Pd to Pt had a marked effect on activity. All catalysts showed an initial peak of activity, and for the low loadings of Pd, the catalysts stabilised at a lower activity. Catalysts with >0.4% Pd were the most active but showed a steady decline in activity, which would limit their long-term application. In view of this, we selected 0.4% Pd as the baseline to add Pt (Figure 5). Again, adding small amounts of Pt to Pd enhanced the activity markedly, but again the most active catalysts showed significant loss of activity after longer time online. Based on the data from these two studies, we selected a bimetallic composition of 0.1% Pt/0.4% Pd on which to base future catalyst design efforts to find a stable catalyst.

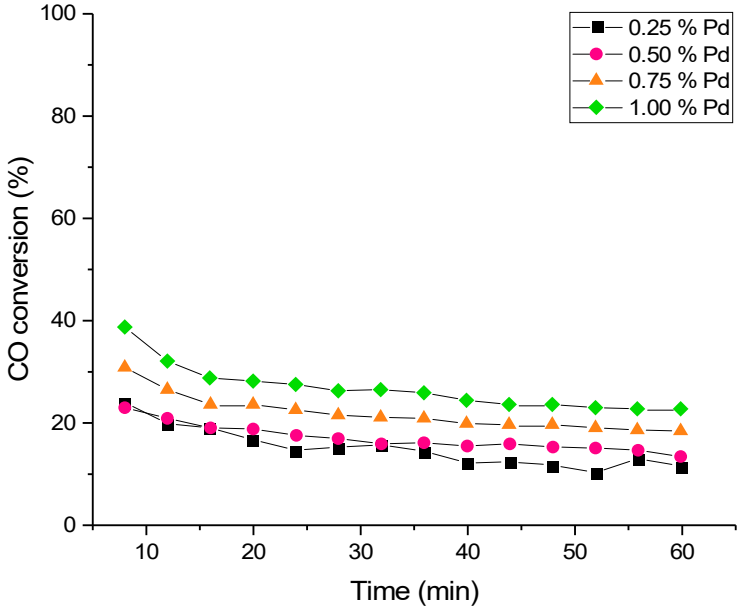

Figure 1. The effect of Pd loading on CO oxidation over Pd/Al_2O_3. Reaction conditions: 25 °C; 1 g catalyst; 25 mL min^{-1} CO (5000 ppm), O_2 (21%), N_2 balance; GHSV = 1500 h^{-1}.

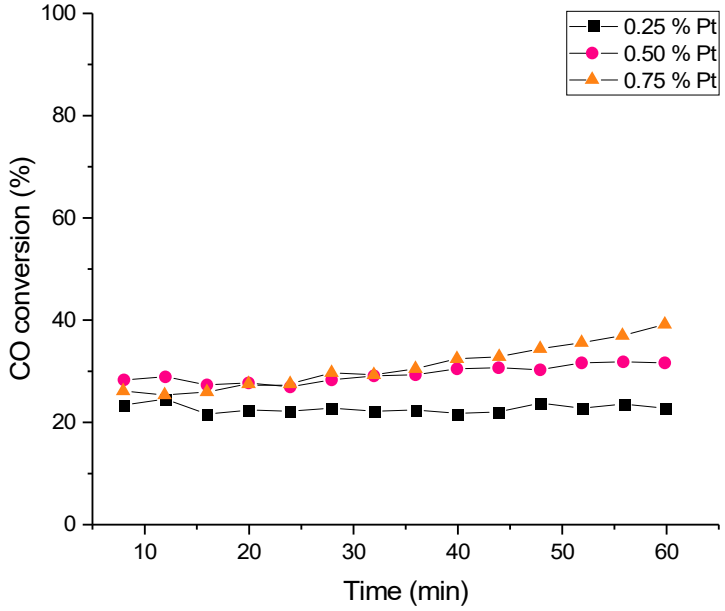

Figure 2. The effect of Pt loading on CO oxidation over Pt/Al_2O_3. Reaction conditions: 25 °C, 1 g catalyst, 25 mL min^{-1} CO (5000 ppm), O_2 (21%), N_2 balance; GHSV = 1500 h^{-1}.

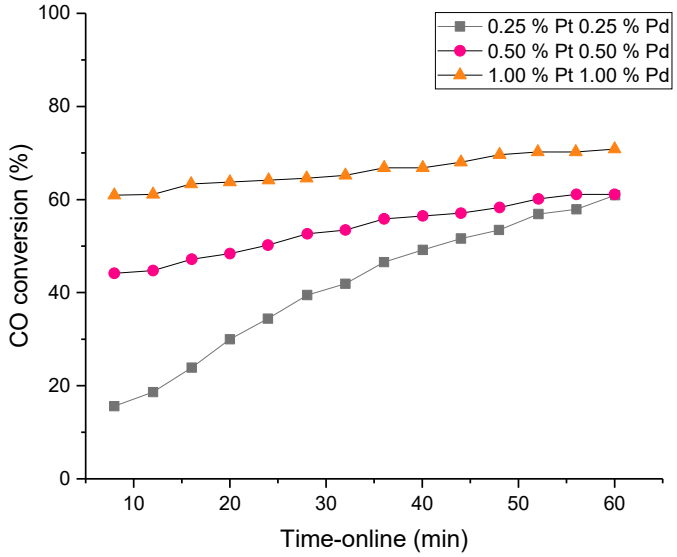

Figure 3. The effect of PtPd loading on CO oxidation over $PtPd/Al_2O_3$. Reaction conditions: 25 °C, 1 g catalyst, CO (5000 ppm), O_2 (21%), N_2 balance; GHSV = 1500 h^{-1}.

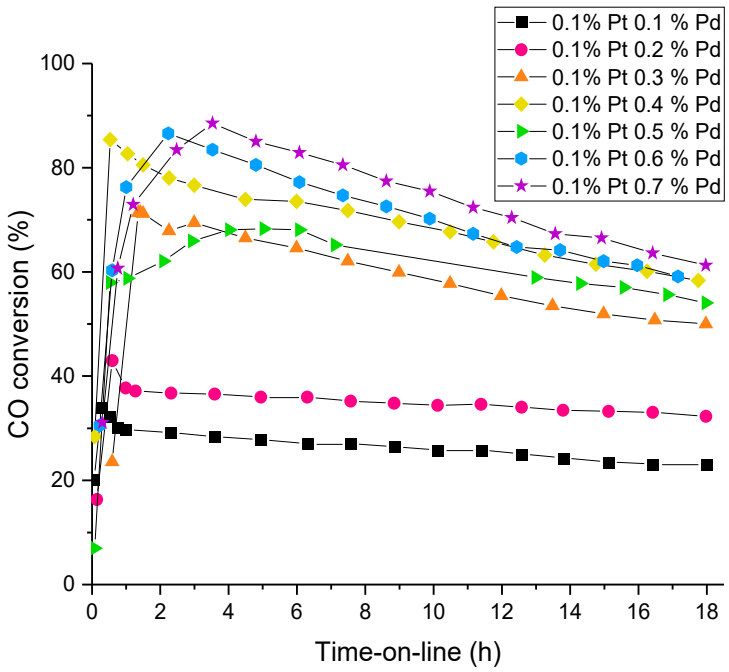

Figure 4. The effect of Pd loading on CO oxidation for 0.1% Pt/0.X% Pd/Al_2O_3 catalysts. Reaction conditions: 25 °C, 1 g catalyst, 25 mL min^{-1} CO (5000 ppm), O_2 (21%), N_2 balance; gas hourly space velocity (GHSV) = 1500 h^{-1}.

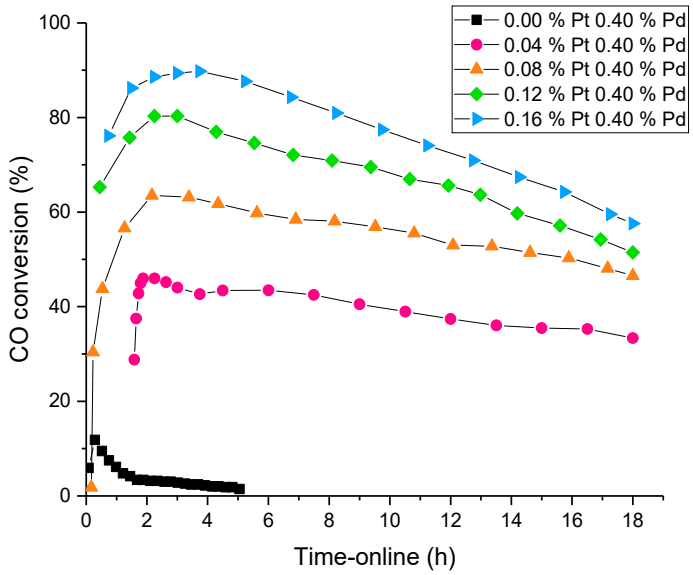

Figure 5. The effect of Pt loading on CO oxidation for 0.1% Pt/0.X% Pd/Al_2O_3 catalysts. Reaction conditions: 25 °C, 1 g catalyst, 25 mL min^{-1} CO (5000 ppm), O_2 (21%), N_2 balance; GHSV = 1500 h^{-1}.

2.2. CO Oxidation Using Bimetallic PtPd Catalysts Supported on Tin Oxide-Coated γ-Alumina Spheres

In an attempt to further increase the catalytic activity without increasing the precious metal content, alumina spheres were coated with tin oxide. The tin oxide-coated alumina spheres were prepared using three different tin compounds and then investigated as support materials for bimetallic PtPd catalysts. It should be noted that all catalysts were prepared, characterised and tested as eggshell formulations using alumina spheres with a diameter of ca. 2 mm. Due to the importance of ambient temperature CO oxidation catalyst for life support applications and the commercial availability of the alumina spheres, we considered it crucial to study the performance of the materials under realistic operating conditions. Whilst the majority of catalytic studies reported in the literature were performed with powdered or sieved materials, allowing a much higher gas hourly space velocity (GHSV) to be reached, it was considered important to evaluate the performance of the spherical supported catalysts under similar conditions to those used in real-life applications. γ-Al_2O_3 spheres were coated with aqueous SnO_2 slurry, corresponding to 0.5, 1, 2, 4, 8 and 16% weight tin loading. After calcination, the spheres were loaded with 0.1% Pt and 0.4% Pd through an electrostatic adsorption (EA) procedure, followed by reduction with sodium formate. The catalysts were tested for ambient temperature CO oxidation. Full conversion was observed across all tin-loaded catalysts at a GHSV of 1500 h^{-1}, showing an enhancement in ambient temperature CO oxidation upon the addition of tin to the catalysts regardless of the precursor; thus, the tin-modified catalysts were tested at a higher GHSV of 3000 h^{-1}. The enhancement in catalytic activity observed upon the addition of tin is likely due to the reducibility of SnO_2. The addition of a reducible support material has been reported to increase oxygen mobility, thus leading to higher activities compared with inert support materials, such as alumina [23,24]. Additionally, the active oxygen species in SnO_2 have been reported to increase SMSI effects, which may also account for an increase in activity [25].

The effect of tin loading on activity for the catalysts prepared from the tin oxide slurry are shown in Figure 6, with the 8% Sn catalyst resulting in the highest activity at ~50% conversion after 12 h. With the exception of the 8% Sn catalyst, all materials prepared from the slurry showed similar conversion levels over a reaction period of 12 h, with no noticeable correlation between tin loading and catalytic activity.

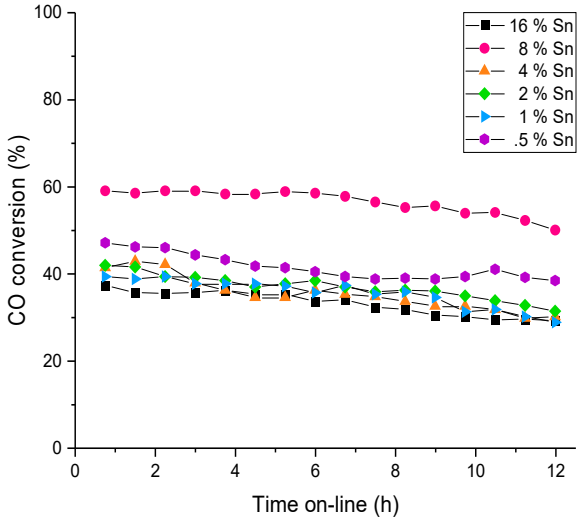

Figure 6. The effect of Sn loading on CO oxidation activity over 0.1% Pt/0.4% Pd/SnO_2/Al_2O_3 catalysts. Reaction conditions: 25 °C, 1 g catalyst, 50 mL min^{-1} CO (5000 ppm), O_2 (21%), N_2 balance; GHSV = 3000 h^{-1}.

Next, we treated the γ-Al_2O_3 spheres with sodium stannate and prepared the catalysts in a similar manner, and the ambient temperature CO oxidation activity is shown in Figure 7. The 1% Sn catalyst was the most active with a steady ~100% conversion for 12 h, showing that this approach has some efficacy. We also made a series of catalysts using tin oxalate (Figure 8), and again it is clear that stable high-activity catalysts could be synthesised using this method. It is interesting that the catalysts prepared using the three tin precursors showed very different trends when the highest activity was plotted against the tin concentration (Figure 9). It is clear that when using sodium stannate or tin oxalate, the dependency on the tin concentration was very different. For the catalysts prepared from sodium stannate, lower levels of tin were found to be most beneficial to catalytic activity, whereas catalytic activity generally increased in line with increasing tin loading for the catalysts prepared from tin oxalate. To gain an understanding of this effect, the catalysts were characterised using X-ray photoelectron spectroscopy (XPS) and energy-dispersive X-ray spectroscopy (EDX).

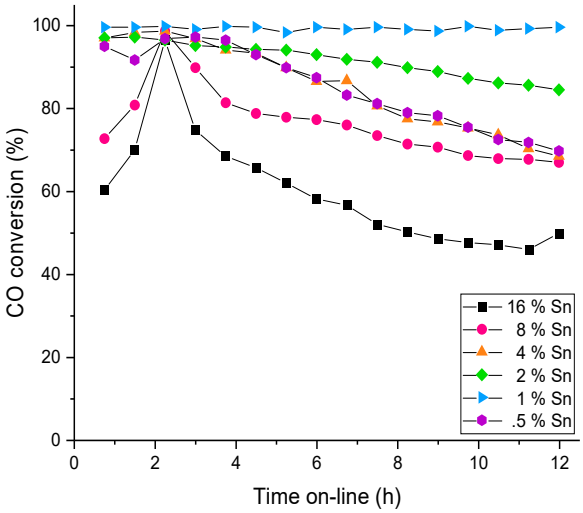

Figure 7. The effect of Sn loading on CO oxidation activity over 0.1% Pt/0.4% Pd/Na_2SnO_3/Al_2O_3 catalysts. Reaction conditions: 25 °C, 1 g catalyst, 50 mL min^{-1} CO (5000 ppm), O_2 (21%), N_2 balance; GHSV = 3000 h^{-1}.

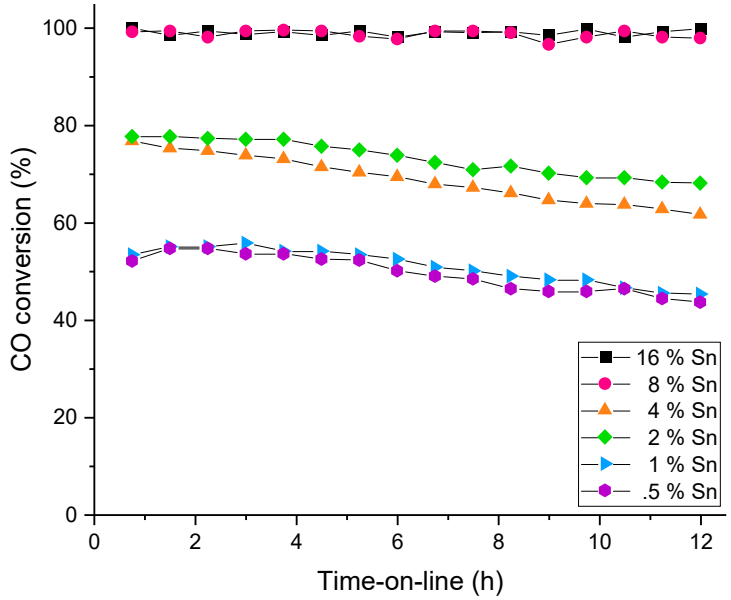

Figure 8. The effect of Sn loading on CO oxidation activity over 0.1% Pt/0.4% Pd/SnC_2O_4/Al_2O_3 catalysts. Reaction conditions: 25 °C, 1 g catalyst, 50 mL min^{-1} CO (5000 ppm), O_2 (21%), N_2 balance; GHSV = 3000 h^{-1}.

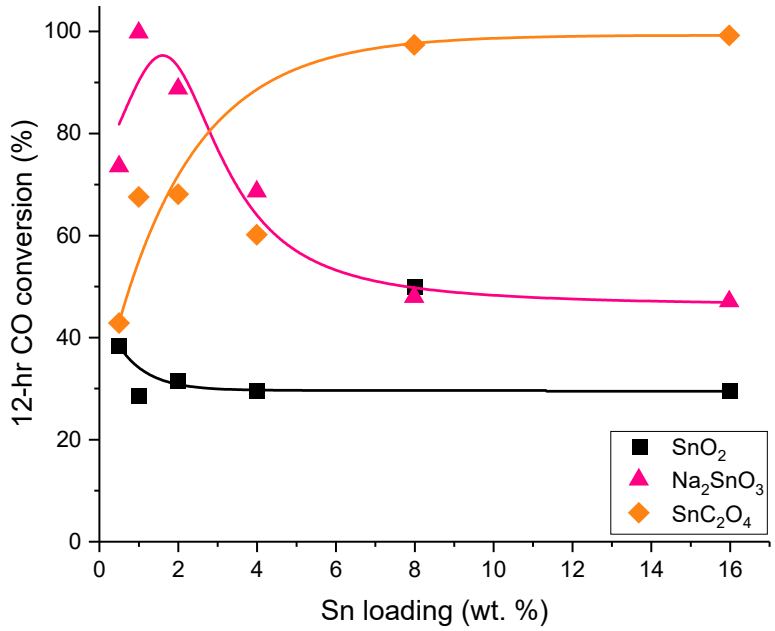

Figure 9. The effect of tin loading on the 12 h catalytic activity of 0.1% Pt/0.4% Pd/SnO_2/Al_2O_3 derived from various tin sources. Reaction conditions: 25 °C, 1 g catalyst, 50 mL min^{-1} CO (5000 ppm), O_2 (21%), N_2 balance; GHSV = 3000 h^{-1}.

2.3. Catalyst Characterisation

Table 1 shows the XPS-derived atomic surface concentrations, whilst Figure 10 shows an expanded section of the survey spectra for the PtPd/SnO_2/Al_2O_3 catalysts. Each spectrum represents the three different Sn precursors for the best and worst performing catalysts with regions for elements of interest highlighted. The full range survey spectra are given in supplementary information (Figure S1).

Table 1. X-ray photoelectron spectroscopy (XPS)-derived atomic concentrations for each catalyst.

Catalyst	Pd	Pt	Sn	O	Al	C	Ca	Pt/Pd Ratio	Dispersion (Sn/Al)
0.1% Pt/0.4% Pd/8% SnO_2/Al_2O_3 (Slurry)	0.80	0.20	0.77	39.72	36.27	21.79	0.45	0.25	0.02
0.1% Pt/0.4% Pd/1% SnO_2/Al_2O_3 (Slurry)	1.08	0.37	0.35	54.48	18.04	25.67	0	0.34	0.02
0.1% Pt/0.4% Pd/1% SnO_2/Al_2O_3 (Na_2SnO_3)	11.47	1.11	1.60	47.17	16.00	22.69	0	0.10	0.10
0.1% Pt/0.4% Pd/16% SnO_2/Al_2O_3 (Na_2SnO_3)	3.96	1.11	5.31	48.17	14.73	26.71	0	0.28	0.36
0.1% Pt/0.4% Pd/16% SnO_2/Al_2O_3 ($Sn(C_2O_4)$)	1.58	0.60	0.56	44.78	33.76	18.72	0	0.38	0.02
0.1% Pt/0.4% Pd/0.5% SnO_2/Al_2O_3 ($Sn(C_2O_4)$)	1.33	0.43	11.77	51.80	12.29	22.40	0	0.32	0.96

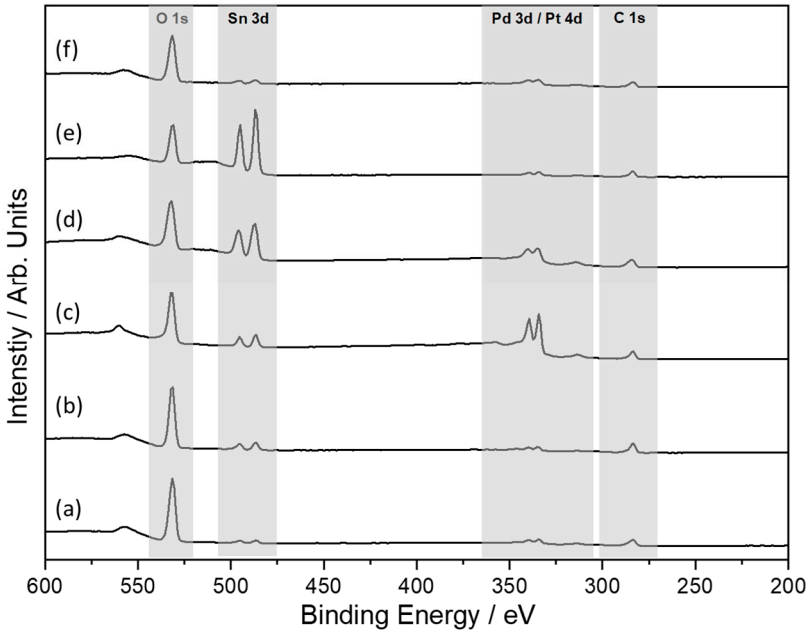

Figure 10. Expansion of a narrow range for the different 0.1% Pt/0.4% Pd/SnO_2/Al_2O_3 catalysts, where (**a**) 1% SnO_2, (**b**) 8% SnO_2, (**c**) 1% SnO_2 from Na_2SnO_3, (**d**) 16% SnO_2 from Na_2SnO_3, (**e**) 0.5% SnO_2 from SnC_2O_4 and (**f**) 16% SnO_2 from SnC_2O_4.

For all catalysts, the percentage of Sn added to the alumina was the same; however, it is clear from Figure 10 that the Sn(3d) signal intensity changed markedly, which is related to the dispersion of Sn, with the most intense signal coming from the lowest-weight loading (Figure 10e), and is attributed to the wetting of the alumina beads by the SnO_2. This difference can be seen by the dispersion ratio reported in Table 1, where a simple approach to evaluating the dispersion is made by taking the corrected Sn intensity divided by the corrected intensity of the Al from the support. Given that the Al signals can always be seen (see Figure S1), it is clear that a thick (>9 nm), continuous SnO_2 film was not present and that island formation was more likely, the dispersion and morphology of which was influenced by the precursor and desired SnO_2 concentration and consistent with Volmer–Weber-type growth for SnO_2 on metal oxides. For example, comparing the SnC_2O_4 precursors, the 0.5% Sn yielded a high Sn surface concentration and dispersion, suggesting a thin film across the surface of the alumina bead, whereas for higher concentrations, island formation dominated due to increased nucleation.

Interestingly for all precursors, the Sn($3d_{5/2}$) energy was found to be 487.7 eV, which is higher than that observed for bulk SnO_2 (ca. 486.5 eV) [35] but consistent with formation of small islands or thin films of SnO_2 [36,37], supporting the XPS results. To illustrate this difference, Figure S2 shows a simple modelling of the photoelectron intensities for different islands by the software SESSA [38].

In all catalysts, both Pd and Pt were present in their metallic states, which we primarily confer by the peak shapes (Figure 11). We took this approach as whilst the binding energy of 335.2 was observed for the Pd($3d_{5/2}$) peak, the corresponding Pt($4f_{7/2}$) peak had a binding energy of 69.4 eV, where the corresponding Pt($4d_{5/2}$) energy was 314.5 eV. The binding energy of the Pt(4f) signal was ca. 1.6 eV lower than that of metallic Pt, and whilst such anomalous values have been observed for PtAu alloys of varying composition and attributed to localisation of s–d bands [39], equally low values have also been observed for Pt supported on Al_2O_3 [40], indicating a possible preferential interaction with the alumina substrate and bimetallic PtSn/Al_2O_3 catalysts. However, given the Pt($4d_{5/2}$) value was consistent with that for metallic Pt, we considered this to be an effect of two distinct charge states, which we attributed to regions of different thicknesses (or island sizes) of SnO_2 as implied by the Sn($3d_{5/2}$) binding energy discussed previously [41–43]. Assuming an ideal Pt/Pd ratio of 0.25 based on the metal loadings, then no direct correlation with Pt/Pd ratio and activity was observed, suggesting that dispersion of the metals may be more optimum and that the preparation method of each SnO_2 coating yields different surface areas, thus influencing the nature of metal deposition.

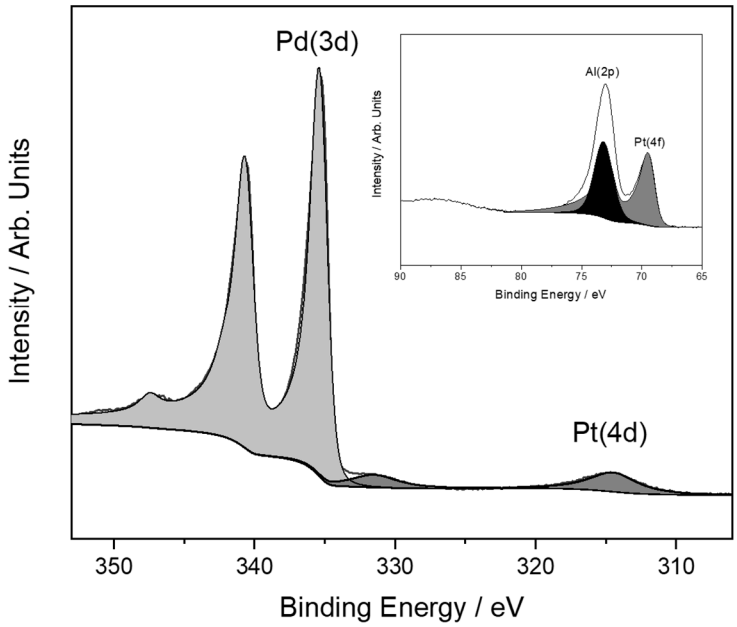

Figure 11. Pd(3d)/Pt(4d) spectra from the 0.5% SnO_2 from SnC_2O_4 with insert showing the corresponding Pt(4f)/Al(2p) spectra representative of all samples. Note the spectra are calibrated with respect to C(1s) at 284.8 eV, and discussion of binding energies are given in the text.

The composition of the best- and worst-performing catalysts from each tin precursor was also investigated by EDX (Table 2). Discrepancies between the nominal quantity of tin reagent added and the tin content in the bulk structure were observed. This can be rationalised by considering the eggshell formulation of the catalysts. Since the catalysts were prepared from large (ca. 2 mm diameter) spheres, the "core" of the materials comprised alumina, with SnO_2, Pt and Pd species impregnated on the surface of the alumina support. As a bulk technique, the EDX results showed the major component of the catalyst to be alumina, although a large proportion of this was confined within the volume of the spheres due to their large diameter.

Table 2. Energy-dispersive X-ray spectroscopy (EDX)-derived weight percentages for each catalyst.

Catalyst	Pd	Pt	Sn	O	Al	Cl	Na	Pt/Pd Ratio
0.1% Pt/0.4% Pd/8% SnO_2/Al_2O_3 (Slurry)	0.30	0.05	1.90	74.39	23.36	N.D.	N.D.	0.16
0.1% Pt./0.4% Pd/1% SnO_2/Al_2O_3 (Slurry)	0.30	0.08	2.45	71.17	26.00	N.D.	N.D.	0.26
0.1% Pt/0.4% Pd/1% SnO_2/Al_2O_3 (Na_2SnO_3)	1.30	0.14	0.86	70.65	26.65	N.D.	0.41	0.11
0.1% Pt/0.4% Pd/16% SnO_2/Al_2O_3 (Na_2SnO_3)	1.08	0.28	1.91	69.17	26.54	0.16	0.85	0.26
0.1% Pt/0.4% Pd/16% SnO_2/Al_2O_3 ($Sn(C_2O_4)$)	0.28	0.03	1.63	75.72	22.35	N.D.	N.D.	0.11
0.1% Pt/0.4% Pd/0.5% SnO_2/Al_2O_3 ($Sn(C_2O_4)$)	0.27	0.09	1.61	71.88	26.33	N.D.	N.D.	0.33

EDX analysis offered some insights into the effect of tin loading on catalytic activity for the catalysts prepared from sodium stannate precursors. Residual sodium was found in both the highest (1% Sn)- and lowest (16% Sn)-activity catalysts, while residual chlorine was also found in the lowest-performing catalyst. This was expected due to the catalyst preparation method. The 16% catalyst was exposed to a higher concentration of sodium through the stannate precursor, thus corresponding to a proportional increase in chloride concentration to maintain the pH through the use of the EA preparation technique. Chloride has previously been reported as a catalyst poison for $Pt/CeO_2/Al_2O_3$ [40], whereas sodium has been described as a promoter for the catalytic activity of PdO/SnO_2 [44]. Whilst significantly more sodium reagent was added to the 16% catalyst compared to the 1% catalyst, the residual sodium content was only doubled for the 16% catalyst and accompanied by residual chloride that was not present in the 1% catalyst. It is postulated that the effect of sodium promotion in the 16% catalyst was countered by the detrimental effect of residual chloride, resulting in a less active catalyst. A similar argument may explain the relatively high activity observed for the 8% Sn catalyst prepared from the SnO_2 slurry. Whilst no bulk contaminants were observed by EDX, calcium was detected as a surface impurity by XPS. It is possible that calcium acts as a promoter in a similar way to sodium, thus the increased activity may be a result of the surface calcium species present in the material. The catalysts prepared from tin oxalate were found to be free of both surface and bulk contaminants by XPS and EDX analysis, respectively. Interestingly, for this series of catalysts, generally, an increase in activity was observed with an increase in tin loading.

The catalyst testing results, alongside XPS and EDX characterisation, suggest that for $PtPd/SnO_2/Al_2O_3$ catalysts prepared in such a manner so as to be free of impurities, e.g., through oxalate combustion, catalytic activity correlates well with tin oxide loading. Similar results have been presented for $Pd/SnO_2/Al_2O_3$ [45] and $Pt–SnO_2/Al_2O_3$ [25]. The high activity has been attributed to a model based on a reverse spillover mechanism, whereby adsorbed O_2 migrates from the oxide to the metal sites to react with chemisorbed CO. Alternatively, for preparations involving the use of tin salts,

such as sodium stannate, the presence of contaminants, such as sodium and chloride, can significantly influence catalytic activity, complicating the effects of tin loading.

3. Materials and Methods

3.1. Catalyst Preparation

3.1.1. PtPd/Al_2O_3 Spheres

PtPd/Al_2O_3 catalysts were prepared by an electrostatic adsorption technique. Briefly, γ-alumina spheres (ca. 2 mm diameter) were hydrated for 1 h with deionised (DI) water. $PtCl_4$ (0.86 g per 0.25% loading, Aldrich, Gillingham, UK) acidified with 6 drops HCl(aq) (3.33%) was mixed with Na_2PdCl_4 (0.420 mL of 1.131 M per 0.25% loading, Aldrich, Gillingham, UK) in 30.0 mL DI water. The metal salt solution was mixed with the alumina slurry, and dilute HCl(aq) (3.70%) was added dropwise to maintain a pH of 3.15 ± 0.25 for 2 h. Following this, Na_2COOH (0.3 g) was added, and the vessel was sealed and aged for 16 h. Following the aging treatment, the catalyst spheres were filtered and extensively washed with H_2O prior to desiccation for 48 h.

3.1.2. PtPd/SnO_2/Al_2O_3 Spheres

Alumina spheres were combined with a slurry comprising acidified tin oxide (0.51 g per 2.0% loading) in DI water. After thorough mixing, the spheres were desiccated for 48 h prior to impregnation with Pt/Pd as described above.

3.1.3. PtPd/Na_2SnO_3/Al_2O_3

Alumina spheres were combined with a solution of $Na_2SnO_3.3H_2O$ (0.9 g per 2.0% tin loading) in DI water, and mixed for 20 min at room temperature followed by 30 min at 70 °C. After thorough mixing, the spheres were desiccated for 48 h prior to impregnation with Pt/Pd as described above.

3.1.4. PtPd/SnC_2O_4/Al_2O_3

Alumina spheres were combined with a slurry comprising $Sn(C_2O_4)$ (0.7 g per 2.0% tin loading) in H_2O_2(aq) (concentration 0.92% per 2.0% loading). After thorough mixing, the spheres were desiccated for 48 h before subsequent calcination at 350 °C under flowing air for 1 h prior to impregnation with Pt/Pd as described above. All quoted loadings were based on the concentrations used in the catalyst preparation procedures. A wide range of tin loadings was adopted so that it covered a range from below the theoretical monolayer coverage to well above.

3.2. Catalyst Characterisation

A Kratos Axis Ultra DLD system (Kratos Analytical Let, Manchester, UK) was used to collect XPS spectra of the spherical catalyst pellets. The catalysts were analysed as integral spheres to avoid dilution by the core of the alumina. Pellets were analysed using a monochromatic Al Kα X-ray source operating at 140 W (10 mA × 14 kV). Spectra were collected with pass energies of 160 eV for survey spectra and 40 eV for high-resolution scans using step sizes of 1 and 0.1 eV, respectively. The spectrometer was operated in the hybrid mode using a combination of magnetic immersion and electrostatic lenses and acquired over an area of approximately 300 × 700 μm^2. A magnetically confined charge compensation system was used to minimize sample charging, and all spectra were taken with a 90° take-off angle. A base pressure $<5 \times 10^{-9}$ Torr was maintained during collection of the spectra. Data was analysed and quantified using CasaXPS after subtraction of a Shirley-type background using modified Wagner sensitivity factors as supplied by the manufacturer.

EDX analysis was performed on spherical catalyst pellets using a Carl Zeiss EVO-40 scanning electron microscope (SEM) (Zeiss, Cambridge, UK) equipped with an INCA x-sight EDX detector. Calibration was first performed using a cobalt standard. A minimum of three samples from each

catalyst were analysed, with multiple scans of each sample. The results represent the average values from all scans.

3.3. Catalyst Testing

Catalyst testing conditions were selected to assess catalyst performance under typical application conditions. The gas stream was first passed through a humidifier containing deionised water at room temperature, corresponding to a water content of ca. 4%. The gas was subsequently passed through a microreactor, which was placed in an isothermally maintained water bath at 25 °C. One gram of desiccated integral alumina sphere-supported catalyst was placed in a cylindrical fixed bed laboratory microreactor with a diameter of ~7 mm. Gas was fed into the reactor at 25 mL min^{-1} (for $PtPd/Al_2O_3$ catalysts) or 50 mL min^{-1} (for $PtPd/SnO_2/Al_2O_3$ catalysts) using a MKS mass flow controller (MKS, Crewe, Cheshire, UK). This equated to a gas hourly space velocity of 1500 and 3000 h^{-1}, respectively; $PtPd/SnO_2/Al_2O_3$ catalysts were tested at a higher GHSV due to complete conversion across catalysts at 1500 h^{-1}. The volume of catalyst used to calculate the GHSV was that based on the use of the 2 mm alumina supporting spheres; hence, the catalyst bed contained considerable void volume between the macroscopic spheres. The postreaction gas stream was analysed online using a Varian CP-3800 GC equipped with a 1.5 m packed Carbosieve column with sampling every 4.5 min intervals. The GC was calibrated with known concentrations of CO_2. Full conversion was calibrated with 5000 ppm CO_2, which is referred to as total CO_2 counts. CO conversion was calculated as follows:

$$CO\ conversion\ (\%) = \left(\frac{CO_2 counts}{Total\ CO_2\ counts}\right) \times 100$$

Experimental error for CO conversion was calculated to be ±3% for these experiments. Catalyst time online data did not always reach steady state, but the conditions employed did allow differentiation of catalyst performance, and catalysts of this type do not always operate under steady state in their applications.

4. Conclusions

A series of bimetallic $PtPd/Al_2O_3$ catalysts were prepared through an electrostatic adsorption technique and investigated for ambient temperature CO oxidation. It was shown that the bimetallic catalysts were more active than their monometallic counterparts and following investigations into the role of the Pt/Pd ratio, a bimetallic composition of 0.1% Pt/0.4% Pd was selected for further studies. The addition of tin oxide to the alumina-supported PtPd catalysts resulted in increased catalytic activity. Catalysts prepared from sodium stannate and tin oxalate were considerably more active than those prepared from a tin oxide slurry, although significant differences were observed between tin loading and catalytic activity depending on the tin precursor selected. For catalysts prepared from tin oxalate, whereby no surface or bulk impurities were detected, increased catalytic activity was generally correlated with increased tin loading, with the highest activity observed over the 16% Sn catalyst. Alternatively, the catalysts prepared from sodium stannate were found to be most active at lower levels of tin loading, with the 1% Sn catalyst demonstrating the highest activity. Analysis by XPS and EDX showed that the catalysts prepared from sodium stannate contained varying levels of sodium and chloride contaminants depending on the amount of tin reagent added, which may further influence catalytic activity. This highlights the importance of precursor and reagent choice during catalyst synthesis, particularly with regard to known catalyst poisons and promotors.

Supplementary Materials: The following are available online at http://www.mdpi.com/2073-4344/10/11/1223/s1, Figure S1: Full range XPS survey spectra of $PtPd/SnO_2/Al_2O_3$. Figure S2: Simulated spectra illustrating effect of SnO_2 island morphologies.

Author Contributions: Conceptualization, M.H., M.J.C., P.W., S.H.T. and G.J.H.; formal analysis, J.K.A., D.J.M., A.F.C. and L.R.S.; writing—original draft preparation, G.J.H., S.H.T., L.R.S. and D.J.M.; writing—review and

editing, M.H., M.J.C., P.W., S.H.T., G.J.H., L.R.S. and D.J.M.; supervision, S.H.T. and G.J.H.; project administration, S.H.T. and G.J.H. All authors have read and agreed to the published version of the manuscript.

Funding: This research received no external funding.

Conflicts of Interest: The authors declare no conflict of interest.

References

1. Haruta, M.; Tsubota, S.; Kobayashi, T.; Kageyama, H.; Genet, M.J.; Delmon, B. Low-Temperature Oxidation of CO over Gold Supported on TiO_2, α-Fe_2O_3, and Co_3O_4. *J. Catal.* **1993**, *144*, 175–192. [CrossRef]
2. Falsig, H.; Hvolbæk, B.; Kristensen, I.S.; Jiang, T.; Bligaard, T.; Christensen, C.H.; Nørskov, J.K. Trends in the Catalytic CO Oxidation Activity of Nanoparticles. *Angew. Chem. Int. Ed.* **2008**, *47*, 4835–4839. [CrossRef] [PubMed]
3. Royer, S.; Duprez, D. Catalytic Oxidation of Carbon Monoxide over Transition Metal Oxides. *ChemCatChem* **2011**, *3*, 24–65. [CrossRef]
4. Hutchings, G.J.; Mirzaei, A.A.; Joyner, R.W.; Siddiqui, M.R.H.; Taylor, S.H. Effect of preparation conditions on the catalytic performance of copper manganese oxide catalysts for CO oxidation. *Appl. Catal. A Gen.* **1998**, *166*, 143–152. [CrossRef]
5. Krämer, M.; Schmidt, T.; Stöwe, K.; Maier, W.F. Structural and catalytic aspects of sol–gel derived copper manganese oxides as low-temperature CO oxidation catalyst. *Appl. Catal. A Gen.* **2006**, *302*, 257–263. [CrossRef]
6. Brittan, M.I.; Bliss, H.; Walker, C.A. Kinetics of the Hopcalite-catalyzed oxidation of carbon monoxide. *AIChE J.* **1970**, *16*, 305–314. [CrossRef]
7. Alayoglu, S.; Nilekar, A.U.; Mavrikakis, M.; Eichhorn, B. Ru–Pt core–shell nanoparticles for preferential oxidation of carbon monoxide in hydrogen. *Nat. Mater.* **2008**, *7*, 333–338. [CrossRef]
8. Mallat, T.; Baiker, A. Oxidation of Alcohols with Molecular Oxygen on Solid Catalysts. *Chem. Rev.* **2004**, *104*, 3037–3058. [CrossRef]
9. Periana, R.A.; Taube, D.J.; Gamble, S.; Taube, H.; Satoh, T.; Fujii, H. Platinum Catalysts for the High-Yield Oxidation of Methane to a Methanol Derivative. *Science* **1998**, *280*, 560–564. [CrossRef]
10. Gélin, P.; Primet, M. Complete oxidation of methane at low temperature over noble metal based catalysts: A review. *Appl. Catal. B: Environ.* **2002**, *39*, 1–37.
11. Liu, K.; Wang, A.; Zhang, T. Recent Advances in Preferential Oxidation of CO Reaction over Platinum Group Metal Catalysts. *ACS Catal.* **2012**, *2*, 1165–1178. [CrossRef]
12. Lee, C.-H.; Chen, Y.-W. Effect of Basic Additives on Pt/Al_2O_3 for CO and Propylene Oxidation under Oxygen-Deficient Conditions. *Ind. Eng. Chem. Res.* **1997**, *36*, 1498–1506. [CrossRef]
13. Carlsson, P.-A.; Skoglundh, M. Low-temperature oxidation of carbon monoxide and methane over alumina and ceria supported platinum catalysts. *Appl. Catal. B Environ.* **2011**, *101*, 669–675. [CrossRef]
14. Bunluesin, T.; Putna, E.S.; Gorte, R.J. A comparison of CO oxidation on ceria-supported Pt, Pd, and Rh. *Catal. Lett.* **1996**, *41*, 1–5. [CrossRef]
15. Becker, E.; Thormählen, P.; Maunula, T.; Suopanki, A.; Skoglundh, M. Low-temperature activity for CO oxidation over diesel oxidation catalysts studied by High Throughput Screening and DRIFT spectroscopy. *Top. Catal.* **2007**, *42*, 421–424. [CrossRef]
16. Wang, L.; Pu, C.; Xu, L.; Cai, Y.; Guo, Y.; Guo, Y.; Lu, G. Effect of supports over Pd/Fe2O3 on CO oxidation at low temperature. *Fuel Process. Technol.* **2017**, *160*, 152–157. [CrossRef]
17. 1An, N.; Li, S.; Duchesne, P.N.; Wu, P.; Zhang, W.; Lee, J.-F.; Cheng, S.; Zhang, P.; Jia, M.; Zhang, W. Size Effects of Platinum Colloid Particles on the Structure and CO Oxidation Properties of Supported Pt/Fe_2O_3 Catalysts. *J. Phys. Chem. C* **2013**, *117*, 21254–21262.
18. Kim, G.J.; Kwon, D.W.; Hong, S.C. Effect of Pt Particle Size and Valence State on the Performance of Pt/TiO_2 Catalysts for CO Oxidation at Room Temperature. *J. Phys. Chem. C* **2016**, *120*, 17996–18004. [CrossRef]
19. Dong, G.; Wang, J.; Gao, Y.; Chen, S. A novel catalyst for CO oxidation at low temperature. *Catal. Lett.* **1999**, *58*, 37–41. [CrossRef]
20. Qiao, B.; Wang, A.; Yang, X.; Allard, L.F.; Jiang, Z.; Cui, Y.; Liu, J.; Li, J.; Zhang, T. Single-atom catalysis of CO oxidation using $Pt1/FeO_x$. *Nat. Chem.* **2011**, *3*, 634–641. [CrossRef]

21. Bond, G.C.; Molloy, L.R.; Fuller, M.J. Oxidation of carbon monoxide over palladium–tin(IV) oxide catalysts: An example of spillover catalysis. *J. Chem. Soc. Chem. Commun.* **1975**, 796–797. [CrossRef]
22. Kamiuchi, N.; Taguchi, K.; Matsui, T.; Kikuchi, R.; Eguchi, K. Sintering and redispersion of platinum catalysts supported on tin oxide. *Appl. Catal. B: Environ.* **2009**, *89*, 65–72. [CrossRef]
23. Grass, K.; Lintz, H.G. The Kinetics of Carbon Monoxide Oxidation on Tin(IV) Oxide Supported Platinum Catalysts. *J. Catal.* **1997**, *172*, 446–452. [CrossRef]
24. Sheintuch, M.; Schmidt, J.; Lecthman, Y.; Yahav, G. Modelling catalyst—Support interactions in carbon monoxide oxidation catalysed by Pd/SnO2. *Appl. Catal.* **1989**, *49*, 55–65. [CrossRef]
25. Wang, X.; Tian, J.S.; Zheng, Y.H.; Xu, X.L.; Liu, W.M.; Fang, X.Z. Tuning Al_2O_3 Surface with SnO_2 to Prepare Improved Supports for Pd for CO Oxidation. *ChemCatChem* **2014**, *6*, 1604–1611. [CrossRef]
26. Bae, J.; Kim, J.; Jeong, H.; Lee, H. CO oxidation on SnO_2 surfaces enhanced by metal doping. *Catal. Sci. Technol.* **2018**, *8*, 782–789. [CrossRef]
27. Śmiechowicz, I.; Kocemba, I.; Rogowski, J.; Czupryn, K. CO oxidation over Pt/SnO_2 catalysts. *React. Kinet. Mech. Catal.* **2018**, *124*, 633–649. [CrossRef]
28. Margitfalvi, J.L.; Borbáth, I.; Hegedűs, M.; Tfirst, E.; Gőbölös, S.; Lázár, K. Low-Temperature CO Oxidation over New Types of Sn–Pt/SiO_2 Catalysts. *J. Catal.* **2000**, *196*, 200–204. [CrossRef]
29. Margitfalvi, J.L.; Borbáth, I.; Hegedűs, M.; Szegedi, Á.; Lázár, K.; Gőbölös, S.; Kristyán, S. Low temperature oxidation of CO over tin-modified Pt/SiO_2 catalysts. *Catal. Today* **2002**, *73*, 343–353. [CrossRef]
30. Margitfalvi, J.L.; Borbáth, I.; Lázár, K.; Tfirst, E.; Szegedi, A.; Hegedűs, M.; Gőbölös, S. In Situ Characterization of Sn–Pt/SiO_2 Catalysts Used in Low Temperature Oxidation of CO. *J. Catal.* **2001**, *203*, 94–103. [CrossRef]
31. Lázár, K.; Rhodes, W.D.; Borbáth, I.; Hegedüs, M.; Margitfalvi, J.L. Reaction-Induced Transformations in Pt–Sn/SiO_2 Catalysts: In Situ ^{119}Sn Mössbauer Study. *Hyperfine Interact.* **2002**, *139*, 87–96. [CrossRef]
32. Hazlett, M.J.; Moses-Debusk, M.; Parks, J.E.; Allard, L.F.; Epling, W.S. Kinetic and mechanistic study of bimetallic Pt-Pd/Al2O3 catalysts for CO and C3H6 oxidation. *Appl. Catal. B Environ.* **2017**, *202*, 404–417. [CrossRef]
33. Chen, R.; Chen, Z.; Ma, B.; Hao, X.; Kapur, N.; Hyun, J.; Cho, K.; Shan, B. CO adsorption on Pt (111) and Pd (111) surfaces: A first-principles based lattice gas Monte-Carlo study. *Comput. Theor. Chem.* **2012**, *987*, 77–83. [CrossRef]
34. Yu, J.; Zhao, D.; Xu, X.; Wang, X.; Zhang, N. Study on RuO_2/SnO_2: Novel and Active Catalysts for CO and CH4 Oxidation. *ChemCatChem* **2012**, *4*, 1122–1132. [CrossRef]
35. Stranick, M.A.; Moskwa, A. SnO_2 by XPS. *Surf. Sci. Spectra* **1993**, *2*, 50–54. [CrossRef]
36. Cao, X.; Cao, L.; Yao, W.; Ye, X. Structural Characterization of Pd-doped SnO_2 Thin Films Using XPS. *Surf. Interface Anal.* **1996**, *24*, 662–666. [CrossRef]
37. Partridge, J.G.; Field, M.R.; Peng, J.L.; Sadek, A.Z.; Kalantar-zadeh, K.; Du Plessis, J.; McCulloch, D.G. Nanostructured SnO_2 films prepared from evaporated Sn and their application as gas sensors. *Nanotechnology* **2008**, *19*, 125504. [CrossRef]
38. Smekal, W.; Werner, W.S.M.; Powell, C.J. Simulation of electron spectra for surface analysis (SESSA): A novel software tool for quantitative Auger-electron spectroscopy and X-ray photoelectron spectroscopy. *Surf. Interface Anal.* **2005**, *37*, 1059–1067. [CrossRef]
39. Wang, D.; Cui, X.; Xiao, Q.; Hu, Y.; Wang, Z.; Yiu, Y.M.; Sham, T.K. Electronic behaviour of Au-Pt alloys and the 4f binding energy shift anomaly in Au bimetallics- X-ray spectroscopy studies. *AIP Adv.* **2018**, *8*, 065210. [CrossRef]
40. Oran, U.; Uner, D. Mechanisms of CO oxidation reaction and effect of chlorine ions on the CO oxidation reaction over Pt/CeO2 and Pt/CeO2/γ-Al2O3 catalysts. *Appl. Catal. B Environ.* **2004**, *54*, 183–191. [CrossRef]
41. Tielsch, B.J.; Fulghum, J.E.; Surman, D.J. Differential Charging in XPS. Part II: Sample Mounting and X-ray Flux Effects on Heterogeneous Samples. *Surf. Interface Anal.* **1996**, *24*, 459–468. [CrossRef]
42. Baer, D.R.; Artyushkova, K.; Cohen, H.; Easton, C.D.; Engelhard, M.; Gengenbach, T.R.; Greczynski, G.; Mack, P.; Morgan, D.J.; Roberts, A. XPS guide: Charge neutralization and binding energy referencing for insulating samples. *J. Vac. Sci. Technol. A* **2020**, *38*, 031204. [CrossRef]
43. Balakrishnan, K.; Schwank, J. A chemisorption and XPS study of bimetallic Pt-Sn/Al_2O_3 catalysts. *J. Catal.* **1991**, *127*, 287–306. [CrossRef]
44. Mirkelamoglu, B.; Karakas, G. The role of alkali-metal promotion on CO oxidation over PdO/SnO_2 catalysts. *Appl. Catal. A Gen.* **2006**, *299*, 84–94. [CrossRef]

45. Akın, A.N.; Kılaz, G.; İşli, A.İ.; Önsan, Z.İ. Development and characterization of Pt–SnO_2/γ-Al_2O_3 catalysts. *Chem. Eng. Sci.* **2001**, *56*, 881–888. [CrossRef]